Bioconjugate Chemistry

Article

pubs.acs.org/bc

Monitoring the Multitask Mechanism of *DNase I* Activity Using Graphene Nanoassemblies

Neil M. Robertson,[†] Mustafa Salih Hizir,[†] Mustafa Balcioglu,[†] Muhit Rana,[†] Hasan Yumak,[§] Ozgur Ecevit,[§] and Mehmet V. Yigit*[,†,‡]

[†]Department of Chemistry and [‡]The RNA Institute, University at Albany, State University of New York, 1400 Washington Avenue, Albany, New York 12222, United States

[§]Department of Science, BMCC, City University of New York, 199 Chambers Street, New York, New York 10007, United States

Supporting Information

ABSTRACT: Here we have demonstrated that graphene serves as a remarkable platform for monitoring the multitask activity of an enzyme with fluorescence spectroscopy. Our studies showed that four different simultaneous enzymatic tasks of *DNase I* can be observed and measured in a high throughput fashion using graphene oxide and oligonucleotide nanoassemblies. We have used phosphorothioate modified oligonucleotides to pinpoint the individual and highly specific functions of *DNase I* with single stranded DNA, RNA, and DNA/DNA and DNA/RNA duplexes. *DNase I* resulted in fluorescence recovery in the nanoassemblies and enhanced the intensity tremendously in the presence of sequence specific DNA or RNA molecules with different degrees of amplification. Our study enabled us to discover the sources of this remarkable signal enhancement, which has been used for biomedical applications of graphene for sensitive detection of specific oncogenes. The significant difference in the signal amplification observed for the detection of DNA and RNA molecules is a result of the positive and/or reductive signal generating events with the enzyme. In the presence of DNA there are four possible ways that the fluorescence reading is influenced, with two of them resulting in a gain in signal while the other two result in a loss. Since the observed signal is a summation of all the events together, the absence of the two fluorescence reduction events with RNA gives a greater degree of fluorescence signal enhancement when compared to target DNA molecules. Overall, our study demonstrates that graphene has powerful features for determining the enzymatic functions of a protein and reveals some of the unknowns observed in the graphene and oligonucleotide assemblies with *DNase I.*

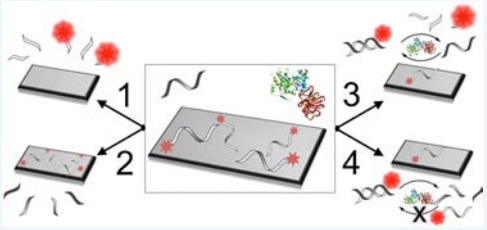

INTRODUCTION

Nanotechnology has been innovating at a remarkable speed over the last few decades. The unique physical properties of the nanoscale materials and their powerful features,[1] particularly in electronic applications, placed them on the production line in a very short period of time. Recent findings demonstrate that nanoscale materials are also extremely useful for monitoring biological events due to their distinct interactions with biomaterials at the bionano interfaces.[2−6] The outstanding features of nanoscale materials for applications in biological and biomedical sciences have attracted researchers to investigate their potential for a variety of biological questions.[7−12] For example, spherical gold nanoparticles have been used for monitoring the natural and unnatural nucleic acid interactions,[13] protein and nucleic acid binding,[14] activity of DNAzymes against specific metal ions,[15−17] structural switching of aptamers with small metabolites,[18,19] and so forth. Moreover, the exceptional potentials of nanomaterials enabled researchers to engineer functional nanoscale devices for the development of biosensors,[20,21] biomedical imaging contrast agents,[22,23] drug delivery vectors,[24−27] and tools for disease diagnosis and therapeutics.[28−30] We have recently performed noninvasive imaging and therapy of breast cancer metastasis in tumor bearing mice by the detection and silencing of a particular overexpressing oncogene with unnatural oligonucleotide functionalized nanoparticles.[30] While the use of three-dimensional spherical nanoparticles has been expanding tremendously, recent findings demonstrate that two-dimensional nanosheets have powerful and distinct features for applications in biology.[31,32]

Graphene oxide (GO) is a one-atom-thick two-dimensional carbon nanomaterial with a honeycomb structure. It is highly dispersed and stable in aqueous solution and has spectacular loading capacity for some of the conventional chemotherapeutic drug molecules due to specific chemical interactions with its large surface area.[33−36] It has been used for the delivery of drug molecules to tumor tissues, detection of cancer biomarkers, and photothermal therapy.[37,38] However, graphene oxide has been an exceptionally useful tool for nucleic acid research.[39] It has a remarkable single stranded oligonucleotide adsorption capacity due to aromatic stacking, hydrophobic interactions, and van der Waals forces between the nucleobases of the oligonucleotides and the graphene surface.[40−42] Moreover, the fluorescence of the fluorophore labels of the

Received: January 30, 2015
Revised: February 24, 2015
Published: March 3, 2015

DOI: 10.1021/acs.bioconjchem.5b00067
Bioconjugate Chem. 2015, 26, 735−745

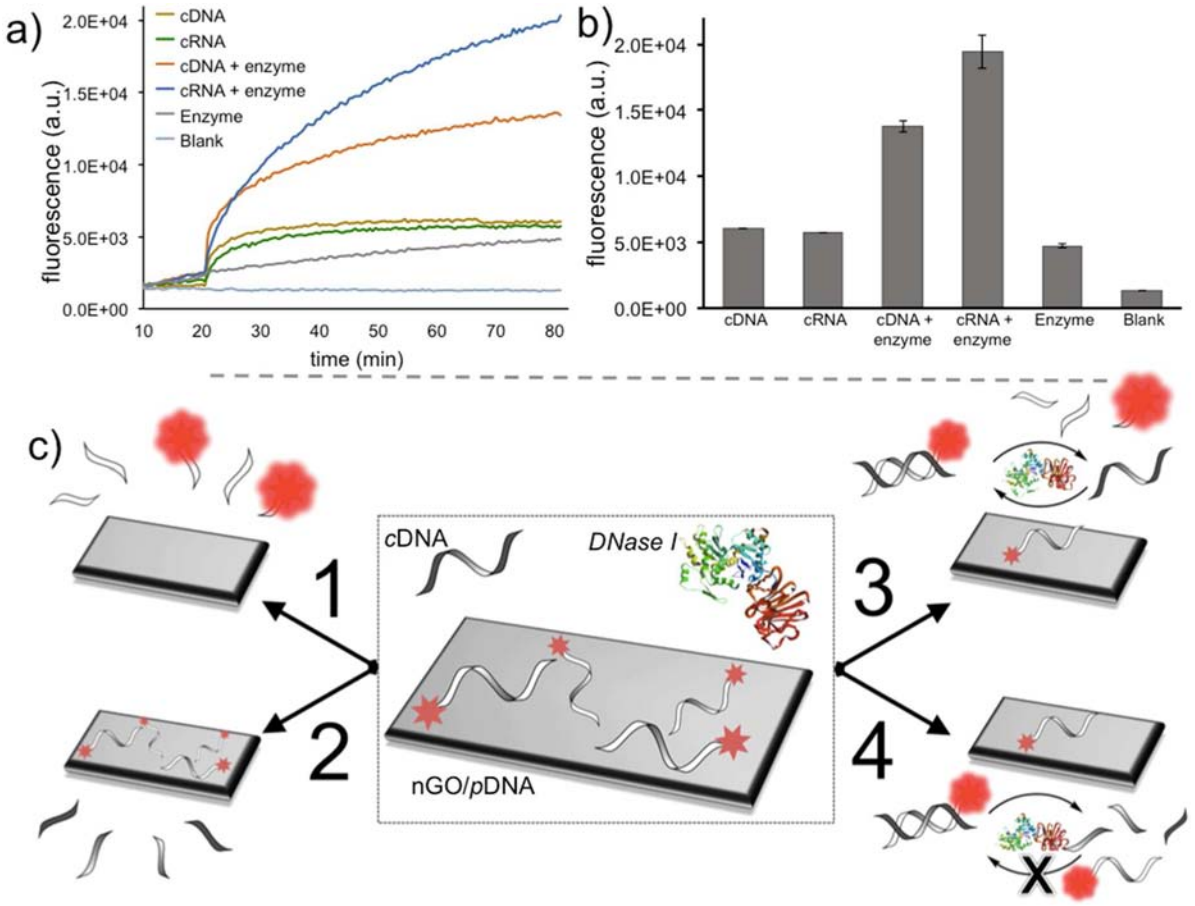

Figure 1. Observed fluorescence recoveries in the presence and absence of *DNase I* and breakdown of the multitask enzymatic activity of *DNase I*. The fluorescence recoveries observed with the addition of *c*DNA, *c*RNA, *c*DNA + *DNase I*, *c*RNA + *DNase I*, or *DNase I* alone to the nGO/*p*DNA nanoassembly (a) by the fluorescence kinetic studies and (b) at the end of the 90 min of incubation. The experiments were performed in triplicate. (c) A schematic representation of the breakdown of the enzymatic activity of *DNase I* and the events in the presence of target strands. (1) The surface adsorbed probe strands, *p*DNA, cleaved by *DNase I*, (2) the target strands, *c*DNA or *c*RNA, cleaved prior to hybridization, (3) the probe strand, *p*DNA, or (4) the target strands, *c*DNA or *c*RNA, cleaved while in the duplex desorbed from the nGO surface. All of these factor into the observed fluorescence measured.

surface adsorbed oligonucleotides can be quenched almost completely resulting in a fluorescently silent GO and single stranded oligonucleotide nanoassembly.[43] On the other hand, in the presence of complementary oligonucleotide strands or DNA binding molecules, the surface adsorbed oligonucleotides are released, resulting in a fluorescence recovery.[44−46] This phenomenon has been used for monitoring nucleic acid interactions,[46,47] detection of miRNAs responsible for various diseases,[28,48] and engineering biosensors with functional oligonucleotides.[45]

The interactions between single stranded oligonucleotides and the graphene surface have been explored in great detail; even recently, Szunerits et al. used surface plasmon resonance (SPR) spectroscopy to study the loading capacity of graphene with single stranded oligonucleotides, gold nanostars, and the functionalized hybrids. They reported that the interactions between the single stranded oligonucleotides and graphene are due to the hydrophobic and/or aromatic stacking of the nucleobases with graphene, which partially deforms the double helix.[49] With regard to adsorption, isothermal titration calorimetry (ITC) measurements have also shown the trend G > A > C > T, which again follows the idea that aromatic stacking affects the adsorption capacity.[50] Along with this, Liu et al. measured the adsorption capacity of single stranded DNA onto the graphene oxide to be 1 μM of DNA per 170 μg mL^{-1} of nGO (8.5 μg mL^{-1} nGO fully loaded with 50 nM of ssDNA).[44]

Although graphene oxide has been heavily utilized for tracing the nucleic acid interactions, it has not been explored for monitoring the enzymatic activity of a protein in depth.[51,52] Here, we have used graphene oxide to monitor the multitask activity of *DNase I* with fluorescence spectroscopy. We have shown that four different simultaneous enzymatic tasks of *DNase I* can be observed and measured in a high throughput fashion using nanosized graphene oxide and oligonucleotide assemblies. Deoxyribonuclease I (*DNase I*) is an important human endonuclease used for the treatment of cystic fibrosis patients.[53,54] Mechanistically, *DNase I* degrades single and double stranded DNA molecules into small fragments by cleaving the phosphodiester bonds in the DNA backbone. It has also been highly utilized for numerous biochemical assays due to its specificity to DNA over RNA. We have used graphene oxide and oligonucleotide nanoassemblies to study some of the very important biochemical functions of *DNase I*. We have demonstrated that graphene oxide is not only a highly versatile platform for monitoring the nucleic acid interactions, but also can be an extremely useful nanomaterial for monitoring the activity of enzymes.

DOI: 10.1021/acs.bioconjchem.5b00067
Bioconjugate Chem. 2015, 26, 735−745

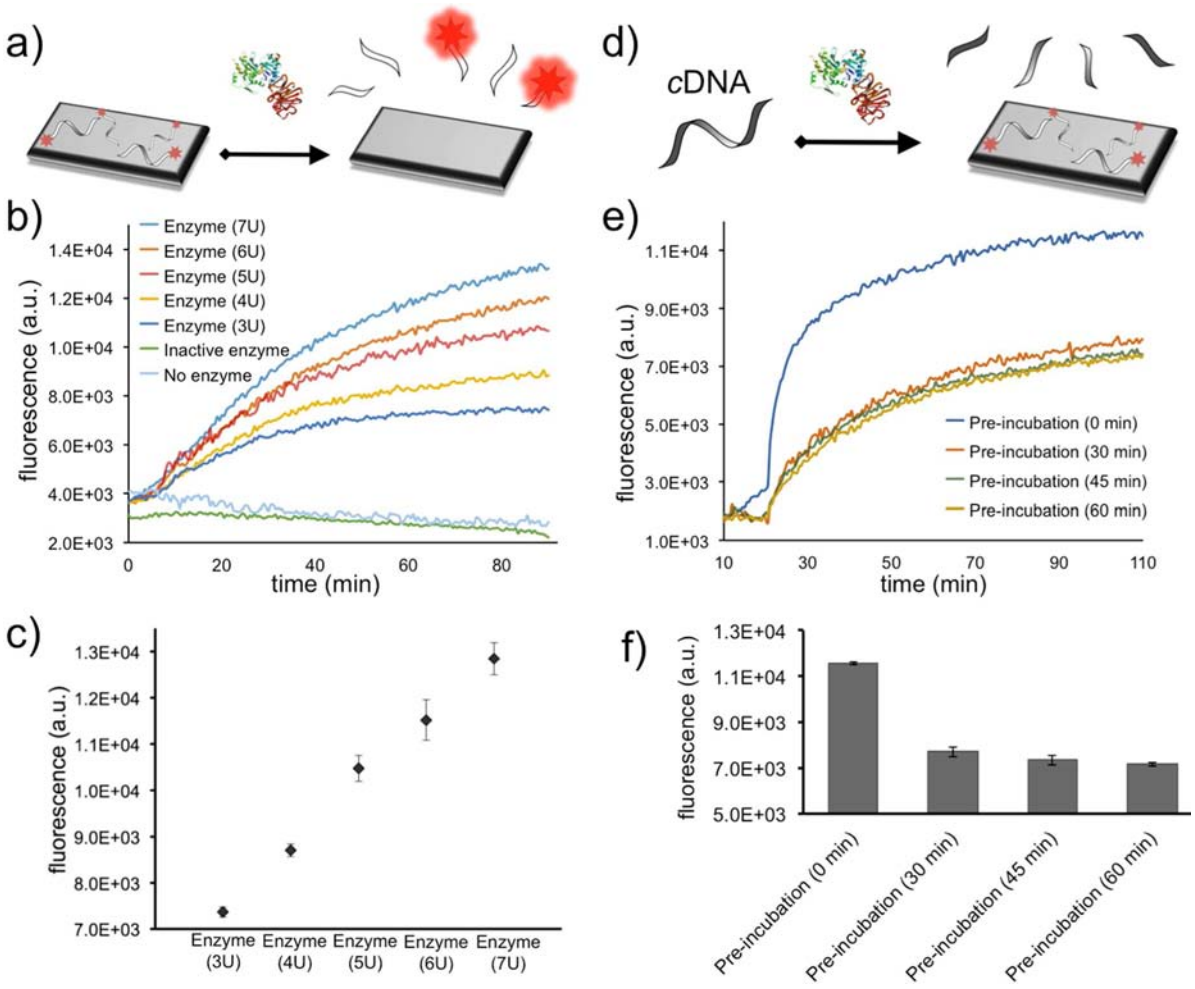

Figure 2. Monitoring the activity of *DNase I* on the surface adsorbed probe ssDNA, *p*DNA, and free target ssDNA, *c*DNA. (a) Schematic representation of the *DNase I* activity on the nGO/*p*DNA nanoassembly. The surface adsorbed *p*DNAs are cleaved by *DNase I*. Fluorescence recoveries observed with various concentrations of *DNase I* at 3, 4, 5, 6, and 7Us of activity (b) by fluorescence kinetic studies and (c) after 90 min of incubation. (d) Schematic representation of the *DNase I* activity on the free *c*DNAs. Cleavage of the *c*DNA strands with 30, 45, and 60 min of preincubation with *DNase I* causes a loss of hybridization and a loss in amplification of total fluorescence observed (e) by kinetic studies and (f) after 90 min of incubation. Experiments were performed in triplicate.

RESULTS AND DISCUSSION

In this study we have used nanosized graphene oxide (nGO) to monitor the activity of an important enzyme, *DNase I*, on various types of natural and unnatural oligonucleotides. We and others have documented that nGO is a superb platform for monitoring nucleic acid interactions.[28,39,43,46] Here, we have demonstrated that nGO is also a very powerful platform for monitoring and understanding the activity of enzymes using fluorescence spectroscopy. Moreover, since some of the nucleases, including *DNase I*, have been used for the detection of low copies of human oncogenes using nGO nanoassemblies with an enhanced fluorescence emission event, it is important to understand the reasoning behind this phenomenon.[55] Our results also enabled us to pinpoint the source of this signal enhancement by the breakdown of the enzymatic tasks of *DNase I* on different types of nucleic acids using graphene.

We first prepared fluorescently silent nGO/*p*DNA nanoassemblies, by adsorbing FAM labeled antisense probe DNA strands (referred to as *p*DNAs) on the nGO surface in order to monitor the activity of *DNase I* (Figure 1c, center). We measured the optimum noncovalent loading density of *p*DNA onto the nGO surface to be 50 nM of *p*DNA per 3 μg/mL of nGO for our construct (Figure S1 and S2). Later, single stranded complementary target RNA or DNA (referred to as *c*RNA and *c*DNA) molecules were used for the desorption of *p*DNAs from the nGO surface through hybridization. As expected, weak fluorescence recoveries were observed in both cases (Figure 1a and b). However, experiments in the presence of *DNase I* showed remarkable signal enhancement with both *c*RNA and *c*DNA over hybridization alone. The fluorescence signals with *c*RNA were much stronger and followed a steeper recovery than *c*DNA. This was expected as the *DNase I* digests only the *p*DNA in the DNA:RNA hybrid and releases *c*RNAs, which can hybridize to another *p*DNA on the surface. On the other hand, both the target and the probe strands in the DNA:DNA duplex are subject to digestion by the enzyme; therefore, the amplification was lower and tends to saturate over time. This is due to the decrease in the concentration of *c*DNAs over time by enzymatic digestion (Figure 1a and b). Along with this saturation, a steady fluorescence signal recovery was observed with *DNase I* alone and the nGO/*p*DNA nanoassembly which was surprising, as single stranded oligonucleotides on the two-dimensional surface were considered to be inaccessible to the enzyme. These observations lead

DOI: 10.1021/acs.bioconjchem.5b00067
Bioconjugate Chem. 2015, 26, 735−745

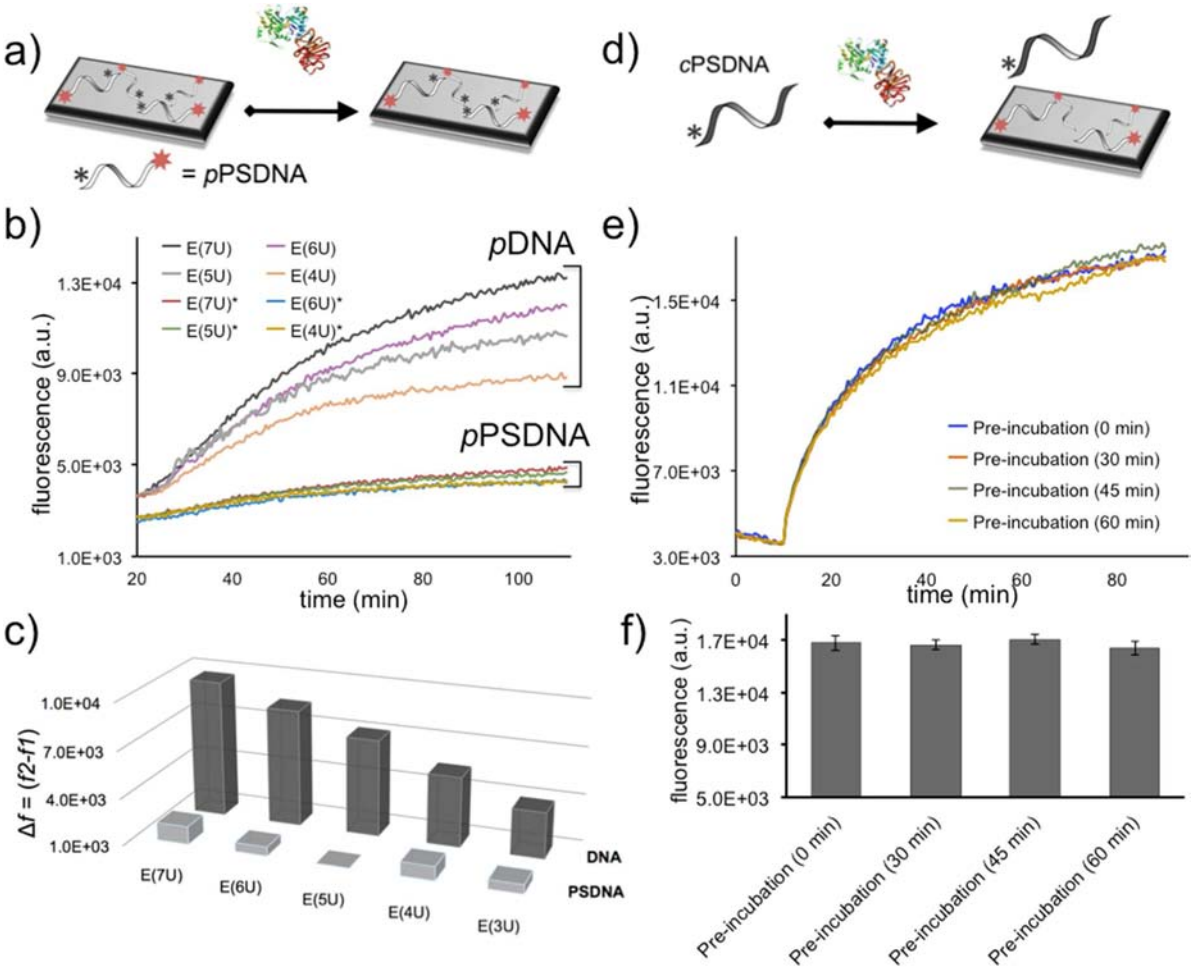

Figure 3. Monitoring the activity of *DNase I* on the surface adsorbed probe and free target oligonucleotides with phosphorothioate modifications. (a) Schematic representation of the *DNase I* activity on the nGO/*p*PSDNA nanoassembly. The surface adsorbed phosphorothioate protected *p*PSDNAs are unable to be cleaved by *DNase I*, observed by fluorescence recoveries with various concentrations of *DNase I* at 4, 5, 6, and 7Us of activity with the nGO/*p*PSDNA nanoassemblies (b) after fluorescence kinetic studies. (c) The difference in the observed fluorescence, Δf, demonstrated the significant signal amplification in the presence of various concentrations of *DNase I* with *p*DNA, but not with *p*PSDNA in the nanoassemblies. (d) Schematic representation of the *DNase I* activity on the free *c*PSDNAs. Since *DNase I* is unable to cleave the protected *c*PSDNA target, there is no loss in amplification of fluorescence with 30, 45, and 60 min of preincubation with *DNase I* observed by (e) fluorescence kinetic studies and (f) after 90 min of incubation. Experiments were performed in triplicate.

us to investigate the mechanism of the *DNase I* activity in detail. We have performed thorough studies to understand the enzymatic activities of *DNase I* on different types of nucleic acids in the nGO and oligonucleotide nanoassemblies.

After performing the kinetic studies with 5 different oligonucleotides and/or enzyme combinations, we proposed four different tasks that *DNase I* could be performing at any given time in the system with *c*DNA (see Figure 1c). In task (1), the *DNase I* acts on the *p*DNA on the surface, cleaving it and therefore increasing the fluorescence signal. In task (2), the *DNase I* acts on the free *c*DNA, cleaving it and decreasing the number of hybridizations and the observed fluorescence signal. In task (3), the *DNase I* acts on the DNA duplex (dsDNA) desorbed from the nGO surface, cleaving the *p*DNA and freeing the *c*DNA to hybridize with another *p*DNA on nGO surface, which results in enhancement of the fluorescence. In task (4), the *DNase I* cleaves the *c*DNA in DNA duplex, which inhibits rehybridization and therefore signal amplification. Since *DNase I* is an endonuclease and only capable of cleaving the DNA strands, the tasks (2) and (4), where there is no fluorescence signal enhancement, are unlikely to occur in the presence of *c*RNA. We first started our systematic investigation on the *DNase I* activity when *c*DNA was used as the target strand to release *p*DNAs from nGO/*p*DNA nanoassembly.

The initial investigation was into the observed activity of *DNase I* on the surface adsorbed *p*DNA, in the nGO/*p*DNA nanoassembly, (task (1), Figure 2a). To investigate this observed activity, the nGO/*p*DNA nanoassembly was incubated with increasing concentrations (3U to 7U) of *DNase I* (Figure 2a). Higher concentrations of *DNase I* resulted in stronger fluorescence signals with greater recovery rates in the nGO/*p*DNA nanoassembly (Figure 2b). Enzymes with a 3U concentration gave the lowest and 7U gave us the highest fluorescence reading at the end of the 90 min of incubation (Figure 2c). In comparison, there was no fluorescence increase at all with no enzyme present or the inactive enzyme (Figure 2b). These results suggest that *DNase I* is capable of cleaving the *p*DNA in the nGO/*p*DNA nanoassembly, which leads to fluorescence recovery that increases over time. For detection of DNA molecules using graphene oxide and *DNase I*-induced signal amplification methods, this type of activity is undesired and can result in false positive results. Moreover, since the

DOI: 10.1021/acs.bioconjchem.5b00067
Bioconjugate Chem. 2015, 26, 735−745

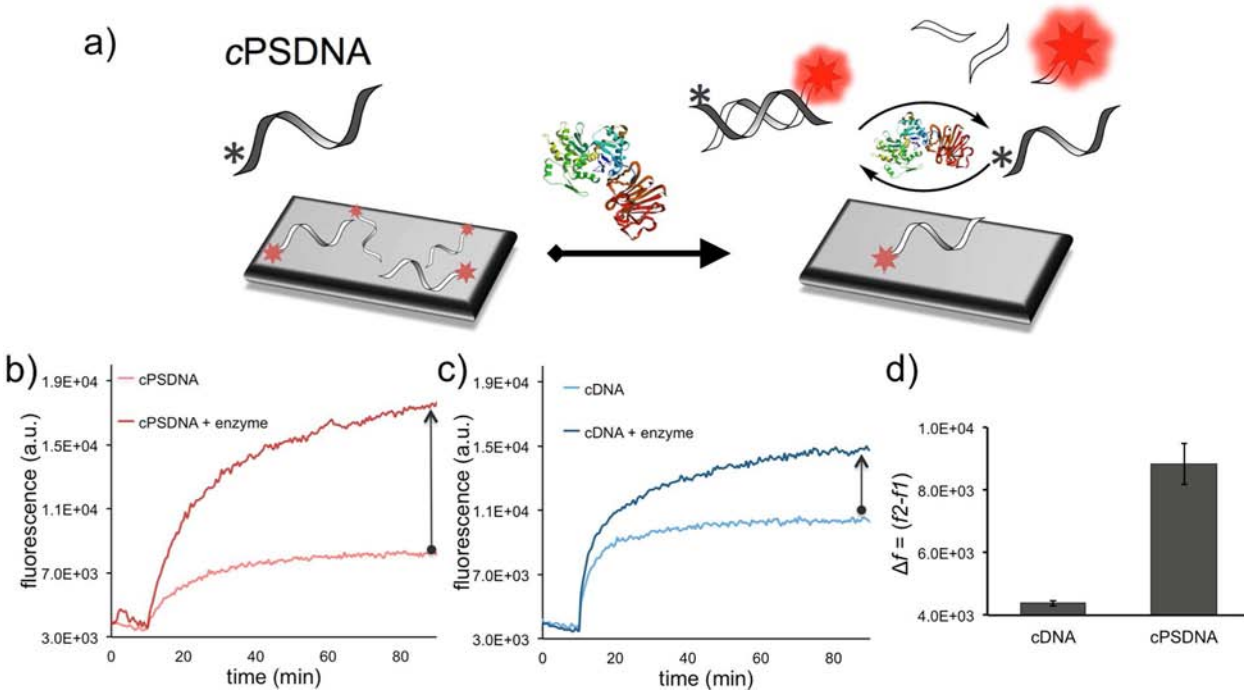

Figure 4. Monitoring the activity of *DNase I* on the target DNA strand (*c*DNA) in the duplex desorbed from the nGO surface. (a) Schematic representation of the *DNase I* activity on the duplex with a phosphorothioate modified target DNA (*c*PSDNA). Due to the cleavage of only the probe strand (*p*DNA) in the duplex, the *c*PSDNA target is then freed and capable of rehybridization to amplify fluorescence. The fluorescence recoveries show that the amplification is greater with (b) phosphorothioate protected sequences (*c*PSDNA) than (c) unprotected sequences (*c*DNA) with *DNase I* after the fluorescence kinetic studies. Arrows show the amplified signals with *c*PSDNA and *c*DNA in the presence of *DNase I*. (d) The difference in the observed fluorescence, Δf, demonstrated the significance of amplification in the presence of *DNase I* when the target strand is protected with phosphorothioate, *c*PSDNA, compared to unprotected target strands, *c*DNA, after 90 min of incubation. Experiments were performed in triplicate.

increase observed in Figure 2b is continuous, the error is amplified over time. After exploring the cleavage of the *p*DNA in the nGO/*p*DNA nanoassembly, we investigated the activity toward the free *c*DNA molecules in solution.

With the possibility of *DNase I* cleaving the free *c*DNA before allowing its hybridization with *p*DNA, the occurrence of task (2) is explored (Figure 2d). Here, the *c*DNA was preincubated with *DNase I* to see if it is cleaved before it can hybridize to *p*DNA in the nGO/*p*DNA nanoassembly. As seen in Figure 2e, changing the preincubation time between 30 and 60 min at 37 °C led to a decreased fluorescence recovery rate when compared to a 0 min incubation. In fact, all preincubated *c*DNA samples were significantly lower than the standard 0 min preincubation (normal addition, no preincubation) (Figure 2f). The results suggest that *DNase I* cleaves the free *c*DNA molecules before they can hybridize and desorb *p*DNAs from the nGO surface and therefore leads to a significant loss in the fluorescence recovery.

After exploring the activity of *DNase I* on the *p*DNAs in the nGO/*p*DNA nanoassembly and free *c*DNA, separately, we moved on to monitor the activity of *DNase I* on the phosphorothioate protected probe and target strands (referred to as *p*PSDNA and *c*PSDNA), individually. The phosphorothioate modification is used to protect the DNA molecules against nuclease cleavage; therefore, we explored the activity of *DNase I* on these modified oligonucleotides using nGO. We first investigated the activity of *DNase I* on the phosphorothioate protected probe strands (*p*PSDNA) in the nGO/*p*PSDNA nanoassembly (Figure 3a). Various concentrations (3U to 7U) of *DNase I* were added to the nGO/*p*PSDNA mixture. As seen in Figure 3b and c, the signals from increasing concentrations of *DNase I* with the nGO/*p*PSDNA nanoassembly are similar to each other and significantly lower when compared to the fluorescence recoveries observed with the unprotected *p*DNA cleavage in the nGO/*p*DNA nanoassembly. This further supports the hypothesis that *DNase I* is active toward surface adsorbed DNA molecules on the two-dimensional graphene surface.

Later we monitored the cleavage of the free *c*PSDNA by *DNase I* before incubation with the nGO/*p*DNA nanoassembly (Figure 3d). The *c*PSDNA was preincubated with *DNase I* for 0 min (normal addition, no incubation) to 60 min at 37 °C followed by the addition of the fluorescently silent nGO/*p*DNA nanoassembly. As seen in Figure 4e and f, regardless of the incubation time with *DNase I*, the observed fluorescence shows no difference. These results show *DNase I* does not cleave *c*PSDNA, but cleaves only the *p*DNAs in the *c*PSDNA:*p*DNA duplex desorbed from the nGO/*p*DNA nanoassembly.

After exploring the activity of *DNase I* on the single stranded DNA states, *p*DNA, *c*DNA, *p*PSDNA, and *c*PSDNA, individually, we performed studies to understand its mechanism of action on the duplexes desorbed from the nGO after hybridization between *p*DNA and *c*DNA. To allow us to monitor these tasks (3) and (4), one of the strands, either *c*DNA or *p*DNA, was protected with phosphorothioate modifications to block the nuclease cleavage on either the target or probe strands.

First, we used *c*PSDNA for desorbing *p*DNAs from the nGO surface to understand task (3) illustrated in Figure 1c. In this event the *c*PSDNA hybridizes with the *p*DNA and releases it

DOI: 10.1021/acs.bioconjchem.5b00067
Bioconjugate Chem. 2015, 26, 735−745

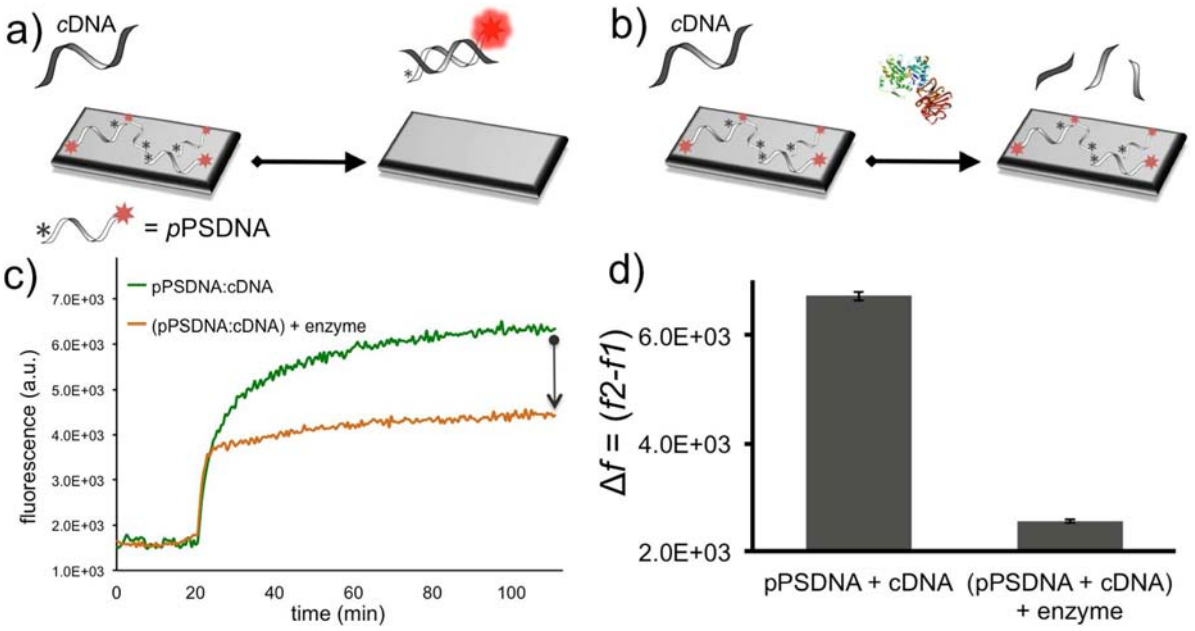

Figure 5. *c*DNA induced fluorescence recovery from the nGO/*p*PSDNA nanoassembly in the (a) absence and (b) presence of *DNase I*. The enzyme reduces hybridization induced fluorescence recovery due to the digestion of the *c*DNA only. Fluorescence recovery with and without *DNase* I observed by (c) fluorescence kinetic studies. (d) The difference in the observed fluorescence, Δf, demonstrated the reduction in fluorescence recovery in the presence of *DNase I* when compared to the enzyme free study at the end of 90 min of incubation. Experiments were performed in triplicate.

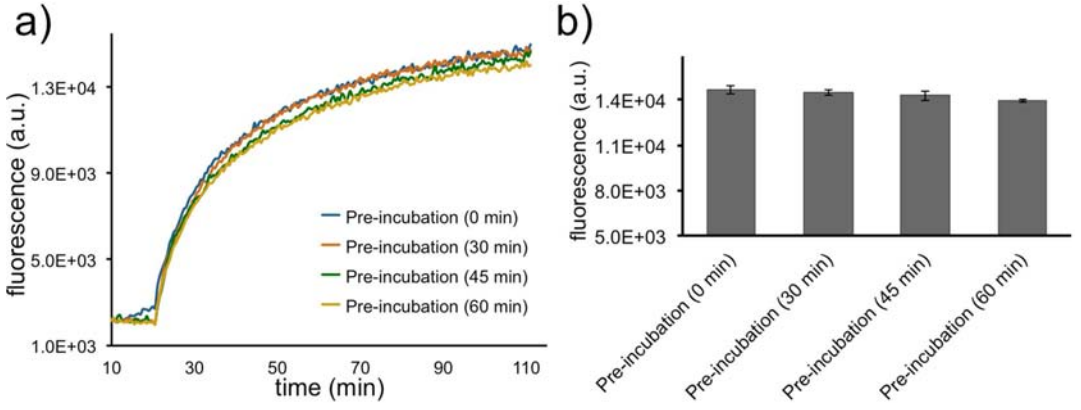

Figure 6. Monitoring the activity of *DNase I* on the free *c*RNA molecules. Since *DNase I* is unable to cleave the protected *c*RNA target, there is no loss in amplification of fluorescence after 30, 45, and 60 min of preincubation with *DNase I* observed by (a) fluorescence kinetic studies and (f) after 90 min of incubation. Experiments were performed in triplicate.

from the nGO/*p*DNA nanoassembly. *DNase I* is now able to cleave the *p*DNA but not *c*PSDNA in the duplex, freeing the *c*PSDNA to hybridize to another *p*DNA from the nGO/*p*DNA nanoassembly, which in turn amplifies the fluorescence recovery (Figure 4a). However, this cleavage is likely to happen on both the probe and target strands if the phosphorothioate modifications were not present. As seen in Figure 4b, *DNase I* induces a significantly enhanced fluorescence recovery with *c*PSDNA. On the other hand this enhancement is not as dramatic with *c*DNA, which is vulnerable to *DNase I* degradation (Figure 3c). As expected, the observed fluorescence recovery with the *c*PSDNA is greater when compared to *c*DNA (Figure 4d). Overall, our results suggest that *DNase I* cleaves the *p*DNAs in the duplexes desorbed from nGO/*p*DNA nanoassembly as proposed in task (3), which as a result enhances the fluorescence signal recovery (Figure 4b). This data also suggests that the cleavage of the probe strands in the duplexes desorbed from nGO and oligonucleotide assemblies is an important component of signal enhancement.

After exploring the activity of *DNase I* on the *p*DNAs in the duplexes, we investigated the activity of *DNase I* on the *c*DNAs in the duplexes desorbed from the nGO/*p*DNA nanoassembly, task (4). For this study the *p*PSDNA was adsorbed on the nGO surface and used to block the activity of enzyme on the probe strands. Therefore, only the *c*DNA target is subject to cleavage, which would lead to a negative impact on the fluorescence recovery due to its enzymatic degradation overtime. The experiments were carried out in the presence and absence of *DNase I* to demonstrate its affect in signal recoveries (Figure 5 scheme). For this study, *c*DNAs were used to release the surface adsorbed *p*PSDNA in the nGO/*p*PSDNA nanoassembly. Figure 5c shows the trends of hybridization induced fluorescence recovery with the *p*PSDNA:*c*DNA duplex in the presence and absence of the enzyme. The loss of fluorescence

DOI: 10.1021/acs.bioconjchem.5b00067
Bioconjugate Chem. 2015, 26, 735−745

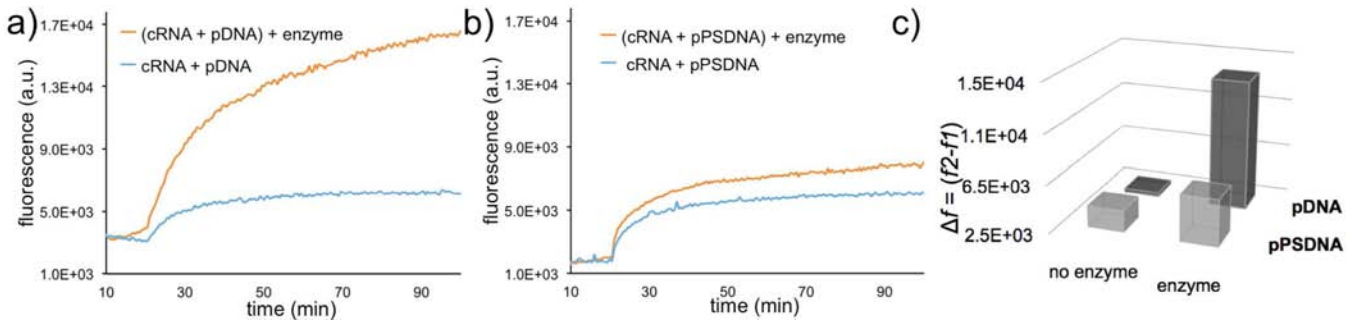

Figure 7. Monitoring the activity of *DNase I* on the *p*DNA:*c*RNA and *p*PSDNA:*c*RNA hybrid recovered using *c*RNA from the surface of the nGO/*p*DNA and nGO/*p*PSDNA nanoassemblies, respectively. Kinetic studies demonstrate that *DNase I* (a) amplifies the signal remarkably in the nGO/*p*DNA nanoassembly; however, (b) does not amplify the signal significantly in the nGO/*p*PSDNA nanoassembly in the presence of *c*RNA (c) The difference in the observed fluorescence, Δ*f*, demonstrated the significance of amplification in the presence of *DNase I* with unprotected probe strands, *p*DNA, when compared to phosphorothioate protected probe strands, *p*PSDNA, after 90 min of incubation. Experiments were performed in triplicate.

in the presence of *DNase I* (Figure 5d) suggests that the enzyme degrades the *c*DNA alone but not *p*PSDNA in the duplexes and decreases the *c*DNA concentration. The actual reduction in fluorescence is observed due to a loss of probe recovery by *c*DNA, as proposed in task (4).

Since all four events involving DNA had been investigated, we monitored the activity of *DNase I* on *c*RNA using nGO. We first tested the activity of *DNase I* against *c*RNA molecules. By replacing *c*DNA with *c*RNA, target strands are resistant to *DNase I* cleavage and therefore higher fluorescence recovery is expected due to the absence of target degradation. To test this event (2), *c*RNA was preincubated with *DNase I* for 0 min (normal addition, no incubation) to 60 min at 37 °C followed by the addition of the fluorescently silent nGO/*p*DNA nanoassembly. As seen in Figure 6a and b, the observed fluorescence had no significant difference regardless of the incubation time of *c*RNA with *DNase I*. These results show *c*RNA as a target is fully protected against *DNase I* and there is a complete loss of target degradation, and in turn no reduction in observed fluorescence.

After demonstrating that free *c*RNA cleavage is not observed, we moved our attention to exploring the action of the enzyme on the *p*DNA:*c*RNA duplex in more detail. As seen in Figure 7a, by using *c*RNA as a target the only molecule for *DNase I* to cleave is *p*DNA, which results in a remarkable signal amplification when compared to *p*DNA:*c*RNA hybridization alone. These data, along with the proven fact that *DNase I* is inactive toward RNA molecules, suggest that *DNase I* does not degrade RNA molecules. The lack of *c*RNA degradation, and ability for it then to recycle with hybridization, gives us the large amplification in fluorescence signal. Knowing we have two different ways to eliminate *DNase I* cleavage, we monitored the *DNase I* activity when both the probe and target strands were protected against *DNase I*. Due to neither of them being cleavable, the initial hypothesis was that the observed fluorescence would only be from hybridization alone. To test this, the *c*RNA was added into the nGO/*p*PSDNA nanoassembly with or without *DNase I*. Figure 7b shows that the observed fluorescence from the hybridization of *p*PSDNA:*c*RNA does not differ greatly from that of *p*PSDNA:*c*RNA in the presence of *DNase I*. The small difference in the recovery is due to the minor replacement of *p*PSDNA by the active enzyme. These results suggest that there would be no cleavage and therefore no amplification when both strands are protected (Figure 7c).

With a detailed investigation of the breakdown of the enzymatic activity of *DNase I* on *c*DNA and *c*RNA molecules with nGO/*p*DNA nanoassemblies completed, we then focused on the degree of fluorescence enhancement with different concentrations of *c*DNA and *c*RNA. Since the digestion of the *c*RNA is not observed by *DNase I*, as suggested by our results, we expected to see significantly higher signal enhancement when compared to *c*DNA. To test our hypothesis, varying concentrations of *c*DNA or *c*RNA (3 nM-50 nM) were added to the nGO/*p*DNA nanoassembly in the presence of *DNase I*. The results after monitoring the observed fluorescence for 3.5 h demonstrate that the *c*RNA results in a significantly larger enhancement than *c*DNA (Figure 8a). By 3.5 h the lowest *c*RNA concentration (3 nM) gives an intensity equal to that of 12 nM *c*DNA and 6 nM of *c*RNA gives an intensity close to 50 nM of *c*DNA, a 4-fold and 8-fold improvement in amplification, respectively (Figure 8b). This significant difference is attributed to the absence of tasks (2) and (4) when RNA is used as a target.

As seen in Figure 8c, in summary tasks (1) and (3) result in the enhancement of the signal with *c*DNA and *c*RNA targets. On the other hand, tasks (2) and (4) result in a signal loss with *c*DNA due its cleavage by the enzyme. However, since *DNase I* is inactive toward *c*RNA molecules, tasks (2) and (4) do not take place with *c*RNA. Therefore, all of the enzymatic actions in the presence of *c*RNA amplify the fluorescence signals. However, the observed signal is a result of two different tasks, with one being considered a background increase, and therefore cannot be used to quantify the RNA concentration precisely.

■ CONCLUSION

We have used nanographene oxide to study the enzymatic activity of *DNase I*, which is a highly specific endonuclease cleaving the phosphodiester linkages in the DNA backbone. We have shown that graphene oxide not only is a versatile platform for monitoring the nucleic acid interactions, but also can be an extremely useful tool for studying the detailed activity of enzymes. We have used modified and/or unmodified nucleic acids and graphene oxide nanoassemblies to pinpoint the specific enzymatic functions of *DNase I*. Also, we have addressed some of the unknowns in fluorescence amplification approaches used for the highly sensitive detection of nucleic acids using *DNase I*. Enzymatic amplification for the sensitive detection of DNA and RNA is an attractive tool for biomedical

DOI: 10.1021/acs.bioconjchem.5b00067
Bioconjugate Chem. 2015, 26, 735−745

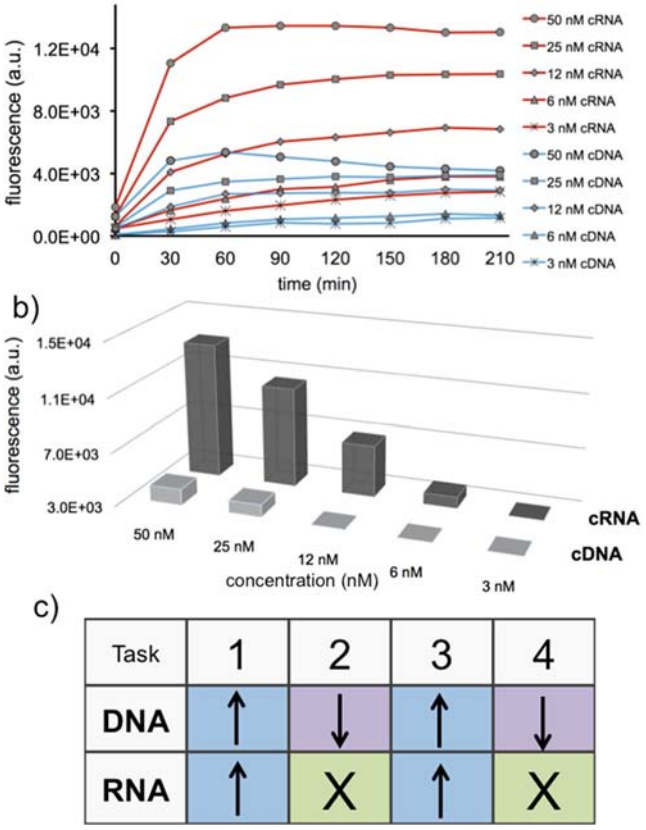

Figure 8. Observed fluorescence recoveries with various concentrations of *c*RNA and *c*DNA in the presence of *DNase I*. The fluorescence recoveries observed with (a) 50, 25, 12, 6, and 3 nM of *c*RNA or *c*DNA at minutes 0, 30, 60, 90, 120, 150, 180, and 210 and (b) at the end of the 210 min of incubation. The experiments were performed in triplicate. (c) Table summarizing the effect of the proposed events (*DNase I* tasks **1**, **2**, **3**, and **4**) on the observed cumulative fluorescence using *c*DNA or *c*RNA as targets. Upward and downward arrows demonstrate the increase and reduction in the fluorescence or signal amplification, respectively. The X represents an absence of the event entirely.

application, and by better understanding the possible mechanism involved, we can better tune the system for optimum results. As we have demonstrated here, there is a significant difference in the observed fluorescence with specific single stranded DNA and RNA targets, which is a result of the positive and/or reductive signal generating events. In the case of DNA there are four possible ways that the fluorescence reading is influenced, with two of them resulting in an enhancement of the signal while the other two result in a decrease. Since the measured fluorescence signal intensity is a summation of all the events together, by the absence of the two fluorescence reduction events with an RNA target, we observe a larger fluorescence when compared to DNA. Our results suggest that even though *DNase I* has been used for the sensitive detection of nucleic acids with an enzymatic amplification approach, it is actually not the best candidate due to the increasing background signal with time from nonspecific cleavage of probe DNA strands on the nGO surface. Other enzyme candidates need to be explored to remove this activity on the surface and open the door for future work.

METHODS

Materials and Reagents. All DNA and RNA sequences were purchased from Integrated DNA Technologies (IDT), USA, with the following sequence information:

(1) FAM-labeled probe DNA (*p*DNA), 5′-/FAM/CACA-AATTCGGTTCTACAGGGTA-3′
(2) Target DNA (*c*DNA), 5′-TACCCTGTAGAACCGA-ATTTGTG-3′
(3) Target RNA (*c*RNA), 5′-UACCCUGUAGAACCGAAU-UUGUG-3′
(4) FAM-labeled phosphorothioate modified probe DNA (*p*PSDNA), 5′-/FAM/C*A*C*A*A*A*T*T*C*G*G*-T*T*C*T*A*C*A*G*G*G*T*A*T-3′
(5) Phosphorothioate modified target DNA (*c*PSDNA), 5′-T*A*C*C*C*T*G*T*A*G*A*A*C*C*G*A*A*-*T*T*T*G*T*G*T-3′

DNase I was purchased from Thermo Fisher Scientific (Waltham, MA, USA) and supplied with 10× reaction buffer (RNase-free, 100 mM Tris-HCl, pH 7.5 at 25 °C, 25 mM $MgCl_2$, 1 mM $CaCl_2$). Carboxyl graphene oxide water dispersion was purchased from ACS Material (Medford, MA, USA) and sonicated 12 h before use, which resulted in a highly stable nanosized graphene oxide (nGO) solution. The average particle size and the zeta potential were determined to be 283.3 ± 15 nm and −23.7 ± 2.9 mV, respectively, using Malvern Instruments Zetasizer Nano ZS. Absorbance measurements were performed using Cary 60 UV−vis Spectrophotometer (Agilent Technologies, Inc., USA). Nuclease-free water was used in preparation of all solutions.

Monitoring *DNase I* Activity on the nGO and Oligonucleotide Nanoassemblies. For initial fluorescence measurements with target oligonucleotides, *c*DNA and *c*RNA, using nanographene oxide (nGO), FAM (ext: 495 nm, emm: 520 nm) labeled antisense DNA molecules, *p*DNA, were used as probe strands. The nGO/*p*DNA nanoassembly was prepared by incubating 3 μg/mL of nGO with 50 nM FAM-labeled *p*DNA in 10 mM Tris-HCl buffer (pH 7.5, 2.5 mM $MgCl_2$, 0.1 mM $CaCl_2$). Briefly, 50 nM of *p*DNA was prepared by diluting a 1 μM stock solution in the Tris-HCl buffer. Later, 1.50 μL of nGO stock solution (200 μg/mL) was added into each 100 μL of 50 nM of *p*DNA solution. The nGO addition resulted in the immediate quenching of fluorescence intensity, with the signal intensity decreased by ∼95%. Observed fluorescence measurements were performed immediately after the sample preparation using a microplate reader. Ten minutes after the initial measurements, 5 μL of 1U/μL stock *DNase I* solution was added to the 100 μL of the nGO/*p*DNA nanoassembly resulting in 5U of *DNase I* activity. At the 20th minute, 2.5 μL of 1 μM (25 nM final) stock solution of *c*DNA or *c*RNA targets were added to the same ∼100 μL mixture containing *DNase I*. A 1.5 h kinetic study at 37 °C was performed to monitor the observed fluorescence and recovery kinetics. For control experiments, samples were run in the absence of 5U of *DNase I*, or *c*DNA or *c*RNA, or without any *DNase I* and target oligonucleotides. The observed fluorescence was obtained with an excitation of 485 nm and an emission of 520 nm.

Activity of *DNase I* on Surface Adsorbed Single Stranded Oligonucleotides. For the detection of *DNase I* activity on the ssDNAs on the nanographene oxide (nGO) surface, *p*DNA was first adsorbed on the nGO surface and then this assembly was treated with *DNase I* alone. The nGO/*p*DNA nanoassembly was prepared by incubating 3 μg/mL of nGO

DOI: 10.1021/acs.bioconjchem.5b00067
Bioconjugate Chem. 2015, 26, 735−745

with 50 nM FAM-labeled *p*DNA in 10 mM Tris-HCl buffer (pH 7.5, 2.5 mM $MgCl_2$, 0.1 mM $CaCl_2$). After the initial fluorescence measurements, 3, 4, 5, 6, or 7 μL of 1U/μL stock *DNase I* was added to the 100 μL of the nGO/*p*DNA nanoassembly resulting in 3U, 4U, 5U, 6U, or 7U of *DNase* I activity. A 1.5 h kinetic study at 37 °C was performed to monitor the observed fluorescence with *DNase I* alone. Control experiments were performed by monitoring the fluorescence after the addition of 5 μL of inactive *DNase I*, heated to 95 °C for 30 min, and with no enzyme addition.

For monitoring the digestion of phosphorothioate modified probe strands, *p*PSDNA, on the nGO surface, a similar approach was performed. Briefly, the nGO/*p*PSDNA nanoassembly was prepared by incubating 3 μg/mL of nGO with 50 nM FAM-labeled *p*PSDNA in 10 mM Tris-HCl buffer (pH 7.5, 2.5 mM $MgCl_2$, 0.1 mM $CaCl_2$). The assembly was then treated with *DNase* I in a similar fashion.

Cleavage of the Single Stranded Target Oligonucleotides by *DNase I* before Addition to nGO and Oligonucleotide Nanoassemblies. For monitoring the cleavage of the ssDNA targets (*c*DNA), the *c*DNA molecules were preincubated with *DNase I*. First, the nGO/*p*DNA nanoassembly was prepared as described above. For preincubation of the *c*DNA with the enzyme, 2.5 μL of a 1 μM (25 nM final) stock *c*DNA was added to 5U of *DNase I* in 10 mM Tris-HCl (pH 7.5, 2.5 mM $MgCl_2$, 0.1 mM $CaCl_2$). The final volume of 10 μL was placed at 37 °C for 30, 45, or 60 min. These preincubated samples were then added to the 100 μL of nGO/*p*DNA nanoassembly in a microplate. The initial fluorescence readings were obtained before the addition of enzyme and *c*DNA mixture, which was followed by a 1.5 h kinetic study at 37 °C to monitor the observed fluorescence after addition of the enzyme and *c*DNA. As a control, a 0 min preincubation was performed where the *c*DNA was not preincubated with 5U of *DNase I*.

For the studies with RNA and phosphorothioate modified target strands, *c*RNA and *c*PSDNA, a similar approach was performed; however, 2.5 μL of a 1 μM stock *c*RNA or *c*PSDNA was used for nuclease digestion instead of *c*DNA.

Monitoring the Cleavage of the Probe Strand in the Surface-Desorbed Duplex by *DNase I*. For monitoring the cleavage of the probe strand in dsDNA desorbed from the nGO surface, as proposed in task (3), the nGO/*p*DNA nanoassembly was prepared as described above. The phosphorothioate modified oligonucleotides (*c*PSDNA) were used as the target sequences for desorbing the surface adsorbed *p*DNA through hybridization. Briefly, to the nGO/*p*DNA nanoassembly, 25 nM of *c*PSDNA was added along with 5U of *DNase I*. A 1.5 h kinetic study at 37 °C was performed to monitor the observed fluorescence. For control and comparison studies, measurements were performed in the absence of *DNase I* or with *c*DNA instead of *c*PSDNA.

Monitoring the Cleavage of the Target Strand in the Surface-Desorbed Duplex by *DNase I*. To monitor the cleavage of the target strand in dsDNA desorbed from the nGO surface, as proposed in task (4), the nGO/*p*PSDNA was prepared as described above. The *c*DNA was used for hybridization induced desorption. To the 100 μL of the nGO/*p*PSDNA, 5U of *DNase I* was added 10 min after the initial measurements. At the 20th minute, 2.5 μL of a 1 μM (25 nM final) stock solution of *c*DNA was added. A 1.5 h kinetic study at 37 °C was performed to monitor the observed fluorescence. Control experiments were performed by monitoring the fluorescence without the addition of *DNase I*. The results were compared with experiments carried out with the nGO/*p*DNA nanoassembly.

Monitoring the *DNase I* Activity on the RNA and Phosphorothioate Modified Oligonucleotide Hybrid Using nGO. The phosphorothioate modified probe strand, *p*PSDNA, was adsorbed onto the nGO forming the nGO/*p*PSDNA nanoassembly. The RNA target, *c*RNA, was used for desorbing the surface adsorbed *p*PSDNA through hybridization. The *DNase I* is inactive to both oligonucleotide types. To the 100 μL of the nGO/*p*PSDNA nanoassembly, 5U of DNase I was added 10 min after the initial fluorescence readings. At the 20th minute, 2.5 μL of 1 μM *c*RNA was added for a 25 nM final concentration. A 1.5 h kinetic study at 37 °C was performed to monitor the observed fluorescence recovery. For control and comparison studies, measurements were performed in the absence of *DNase I* or with *p*DNA instead of *p*PSDNA.

Monitoring the Cumulative Multitask Activity of *DNase I* on Oligonucleotides Using nGO. To measure the cumulative fluorescence signals in tasks (1, 2, 3, and 4) with *DNase I* in the presence of target DNA and RNA molecules, the nGO/*p*DNA nanoassembly was prepared and tested with various concentrations of *c*DNA and *c*RNA at several time points. To 100 μL of the nGO/*p*DNA nanoassembly, 5U of *DNase I* was added. Immediately afterwards 3, 6, 12, 25, and 50 nM final concentrations of *c*DNA or *c*RNA were added into the wells of the microplate. A 3.5 h kinetic study at 37 °C was performed to monitor the observed fluorescence.

Fluorescence Measurements. Fluorescence measurements were performed using a BioTek Synergy H1 microplate reader. For monitoring the fluorescence of the FAM during the kinetic measurements through either nonstop reading or end point reading, the samples were excited at 485 nm and the emission was collected at 520 nm. For each reading, the gain value was set to 100 and the temperature was set to 37 °C for *DNase I* activity.

■ ASSOCIATED CONTENT

Ⓢ Supporting Information

Additional experimental results are provided. This material is available free of charge via the Internet at http://pubs.acs.org.

■ AUTHOR INFORMATION

Corresponding Author

*E-mail: myigit@albany.edu. Tel: (1) 518-442-3002.

Notes

The authors declare no competing financial interest.

■ ACKNOWLEDGMENTS

We would like to thank Profs. Jia Sheng and Maksim Royzen for the discussions on the modified nucleic acids. We would like to thank Ahmad Nazem for the zeta potential and particle size measurements.

■ REFERENCES

(1) Yildirim, A., Acar, H., Erkal, T. S., Bayindir, M., and Guler, M. O. (2011) Template-directed synthesis of silica nanotubes for explosive detection. *ACS Appl. Mater. Interfaces 3*, 4159−4164.

(2) Hamner, K. L., Alexander, C. M., Coopersmith, K., Reishofer, D., Provenza, C., and Maye, M. M. (2013) Using temperature-sensitive smart polymers to regulate DNA-mediated nanoassembly and encoded nanocarrier drug release. *ACS Nano 7*, 7011−7020.

DOI: 10.1021/acs.bioconjchem.5b00067
Bioconjugate Chem. 2015, 26, 735−745

(3) Alam, R., Fontaine, D. M., Branchini, B. R., and Maye, M. M. (2012) Designing quantum rods for optimized energy transfer with firefly luciferase enzymes. *Nano Lett. 12*, 3251−3256.
(4) Alam, R., Zylstra, J., Fontaine, D. M., Branchini, B. R., and Maye, M. M. (2013) Novel multistep BRET-FRET energy transfer using nanoconjugates of firefly proteins, quantum dots, and red fluorescent proteins. *Nanoscale 5*, 5303−5306.
(5) Balcioglu, M., Rana, M., Robertson, N., and Yigit, M. V. (2014) DNA-length-dependent quenching of fluorescently labeled iron oxide nanoparticles with gold, graphene oxide and MoS_2 nanostructures. *ACS Appl. Mater. Interfaces 6*, 12100−12110.
(6) Acar, H., Genc, R., Urel, M., Erkal, T. S., Dana, A., and Guler, M. O. (2012) Self-assembled peptide nanofiber templated one-dimensional gold nanostructures exhibiting resistive switching. *Langmuir 28*, 16347−16354.
(7) Allijn, I. E., Leong, W., Tang, J., Gianella, A., Mieszawska, A. J., Fay, F., Ma, G., Russell, S., Callo, C. B., Gordon, R. E., et al. (2013) Gold nanocrystal labeling allows low-density lipoprotein imaging from the subcellular to macroscopic level. *ACS Nano 7*, 9761−9770.
(8) Mieszawska, A. J., Mulder, W. J., Fayad, Z. A., and Cormode, D. P. (2013) Multifunctional gold nanoparticles for diagnosis and therapy of disease. *Mol. Pharmaceutics 10*, 831−847.
(9) Huang, H., Song, W., Chen, G., Reynard, J. M., Ohulchanskyy, T. Y., Prasad, P. N., Bright, F. V., and Lovell, J. F. (2014) Pd-porphyrin-cross-linked implantable hydrogels with oxygen-responsive phosphorescence. *Adv. Healthc. Mater. 3*, 891−896.
(10) Carter, K. A., Shao, S., Hoopes, M. I., Luo, D., Ahsan, B., Grigoryants, V. M., Song, W., Huang, H., Zhang, G., Pandey, R. K., et al. (2014) Porphyrin-phospholipid liposomes permeabilized by near-infrared light. *Nat. Commun. 5*, 3546.
(11) Ozhalici-Unal, H., and Armitage, B. A. (2009) Fluorescent DNA nanotags based on a self-assembled DNA tetrahedron. *ACS Nano 3*, 425−433.
(12) Benvin, A. L., Creeger, Y., Fisher, G. W., Ballou, B., Waggoner, A. S., and Armitage, B. A. (2007) Fluorescent DNA nanotags: supramolecular fluorescent labels based on intercalating dye arrays assembled on nanostructured DNA templates. *J. Am. Chem. Soc. 129*, 2025−2034.
(13) Rana, M., Balcioglu, M., and Yigit, M. V. (2014) Locked nucleic acid-modified antisense miR-10b oligonucleotides form stable duplexes on gold nanoparticles. *BioNanoScience 139*, 714−720.
(14) Liang, G., Cai, S., Zhang, P., Peng, Y., Chen, H., Zhang, S., and Kong, J. (2011) Magnetic relaxation switch and colorimetric detection of thrombin using aptamer-functionalized gold-coated iron oxide nanoparticles. *Anal. Chim. Acta 689*, 243−249.
(15) Mazumdar, D., Liu, J., Lu, G., Zhou, J., and Lu, Y. (2010) Easy-to-use dipstick tests for detection of lead in paints using non-cross-linked gold nanoparticle-DNAzyme conjugates. *Chem. Commun. 46*, 1416−1418.
(16) Liu, J., and Lu, Y. (2003) A colorimetric lead biosensor using DNAzyme-directed assembly of gold nanoparticles. *J. Am. Chem. Soc. 125*, 6642−6643.
(17) Wei, Q., Nagi, R., Sadeghi, K., Feng, S., Yan, E., Ki, S. J., Caire, R., Tseng, D., and Ozcan, A. (2014) Detection and spatial mapping of mercury contamination in water samples using a smart-phone. *ACS Nano 8*, 1121−1129.
(18) Shi, Y., Dai, H., Sun, Y., Hu, J., Ni, P., and Li, Z. (2013) Fluorescent sensing of cocaine based on a structure switching aptamer, gold nanoparticles and graphene oxide. *Analyst 138*, 7152−7156.
(19) Zhang, J., Wang, L., Pan, D., Song, S., Boey, F. Y., Zhang, H., and Fan, C. (2008) Visual cocaine detection with gold nanoparticles and rationally engineered aptamer structures. *Small 4*, 1196−1200.
(20) Liu, J., and Lu, Y. (2005) Fast colorimetric sensing of adenosine and cocaine based on a general sensor design involving aptamers and nanoparticles. *Angew. Chem., Int. Ed. 45*, 90−94.
(21) Wu, P., Hwang, K., Lan, T., and Lu, Y. (2013) A DNAzyme-gold nanoparticle probe for uranyl ion in living cells. *J. Am. Chem. Soc. 135*, 5254−5257.
(22) Zhang, Y., Jeon, M., Rich, L. J., Hong, H., Geng, J., Zhang, Y., Shi, S., Barnhart, T. E., Alexandridis, P., Huizinga, J. D., et al. (2014) Non-invasive multimodal functional imaging of the intestine with frozen micellar naphthalocyanines. *Nat. Nanotechnol. 9*, 631−638.
(23) Sulek, S., Mammadov, B., Mahcicek, D. I., Sozeri, H., Atalar, E., Tekinay, A. B., and Guler, M. O. (2011) Peptide functionalized superparamagnetic iron oxide nanoparticles as MRI contrast agents. *J. Mater. Chem. 21*, 15157−15162.
(24) Medarova, Z., Pham, W., Farrar, C., Petkova, V., and Moore, A. (2007) In vivo imaging of siRNA delivery and silencing in tumors. *Nat. Med. 13*, 372−377.
(25) Alexander, C. M., Hamner, K. L., Maye, M. M., and Dabrowiak, J. C. (2014) Multifunctional DNA-gold nanoparticles for targeted doxorubicin delivery. *Bioconjugate Chem. 25*, 1261−1271.
(26) Ulasan, M., Yavuz, E., Bagriacik, E. U., Cengeloglu, Y., and Yavuz, M. S. (2014) Biocompatible thermoresponsive PEGMA nanoparticles crosslinked with cleavable disulfide-based crosslinker for dual drug release. *J. Biomed. Mater. Res., Part A 103*, 243−251.
(27) Yavuz, M. S., Cheng, Y., Chen, J., Cobley, C. M., Zhang, Q., Rycenga, M., Xie, J., Kim, C., Song, K. H., Schwartz, A. G., et al. (2009) Gold nanocages covered by smart polymers for controlled release with near-infrared light. *Nat. Mater. 8*, 935−939.
(28) Hizir, M. S., Balcioglu, M., Rana, M., Robertson, N. M., and Yigit, M. V. (2014) Simultaneous detection of circulating OncomiRs from body fluids for prostate cancer staging using nanographene oxide. *ACS Appl. Mater. Interfaces 6*, 14772−14778.
(29) Kumar, M., Yigit, M., Dai, G., Moore, A., and Medarova, Z. (2010) Image-guided breast tumor therapy using a small interfering RNA nanodrug. *Cancer Res. 70*, 7553−7561.
(30) Yigit, M. V., Ghosh, S. K., Kumar, M., Petkova, V., Kavishwar, A., Moore, A., and Medarova, Z. (2013) Context-dependent differences in miR-10b breast oncogenesis can be targeted for the prevention and arrest of lymph node metastasis. *Oncogene 32*, 1530−1538.
(31) Zhu, A. Y., Yi, F., Reed, J. C., Zhu, H., and Cubukcu, E. (2014) Optoelectromechanical multimodal biosensor with graphene active region. *Nano Lett. 14*, 5641−5649.
(32) Guo, Q., Zhu, H., Liu, F., Zhu, A. Y., Reed, J. C., Yi, F., and Cubukcu, E. (2014) Silicon-on-glass graphene-functionalized leaky cavity mode nanophotonic biosensor. *ACS Photonics 1*, 221−227.
(33) Balcioglu, M., Rana, M., and Yigit, M. V. (2013) Doxorubicin loading on graphene oxide, iron oxide and gold nanoparticle hybrid. *J. Mater. Chem. B 1*, 6187−6193.
(34) Wu, J., Wang, Y. S., Yang, X. Y., Liu, Y. Y., Yang, J. R., Yang, R., and Zhang, N. (2012) Graphene oxide used as a carrier for adriamycin can reverse drug resistance in breast cancer cells. *Nanotechnology 23*, 355101.
(35) Zhang, L., Xia, J., Zhao, Q., Liu, L., and Zhang, Z. (2010) Functional graphene oxide as a nanocarrier for controlled loading and targeted delivery of mixed anticancer drugs. *Small 6*, 537−544.
(36) Wang, F., and Liu, J. (2013) Nanodiamond decorated liposomes as highly biocompatible delivery vehicles and a comparison with carbon nanotubes and graphene oxide. *Nanoscale 5*, 12375−12382.
(37) Yang, K., Feng, L., Shi, X., and Liu, Z. (2013) Nano-graphene in biomedicine: theranostic applications. *Chem. Soc. Rev. 42*, 530−547.
(38) Lu, Z., Zhang, L., Deng, Y., Li, S., and He, N. (2012) Graphene oxide for rapid microRNA detection. *Nanoscale 4*, 5840−5842.
(39) Huang, P. J., and Liu, J. (2012) Molecular beacon lighting up on graphene oxide. *Anal. Chem. 84*, 4192−4198.
(40) Manohar, S., Mantz, A. R., Bancroft, K. E., Hui, C. Y., Jagota, A., and Vezenov, D. V. (2008) Peeling single-stranded DNA from graphite surface to determine oligonucleotide binding energy by force spectroscopy. *Nano Lett. 8*, 4365−4372.
(41) Varghese, N., Mogera, U., Govindaraj, A., Das, A., Maiti, P. K., Sood, A. K., and Rao, C. N. (2009) Binding of DNA nucleobases and nucleosides with graphene. *ChemPhysChem 10*, 206−210.
(42) Park, J. S., Na, H. K., Min, D. H., and Kim, D. E. (2013) Desorption of single-stranded nucleic acids from graphene oxide by disruption of hydrogen bonding. *Analyst 138*, 1745−1749.

DOI: 10.1021/acs.bioconjchem.5b00067
Bioconjugate Chem. 2015, 26, 735−745

(43) Liu, B., Sun, Z., Zhang, X., and Liu, J. (2013) Mechanisms of DNA sensing on graphene oxide. *Anal. Chem. 85*, 7987−7993.
(44) Wu, M., Kempaiah, R., Huang, P. J., Maheshwari, V., and Liu, J. (2011) Adsorption and desorption of DNA on graphene oxide studied by fluorescently labeled oligonucleotides. *Langmuir 27*, 2731−2738.
(45) Balcioglu, M., Buyukbekar, B. Z., Yavuz, M. S., and Yigit, M. V. (2015) Smart-polymer-functionalized graphene nanodevices for thermo-switch-controlled biodetection. *ACS Biomater. Sci. Eng. 1*, 27−36.
(46) Rana, M., Balcioglu, M., Robertson, N., and Yigit, M. V. (2014) Nano-graphene oxide as a novel platform for monitoring the effect of LNA modification on nucleic acid interactions. *Analyst 139*, 714−720.
(47) Huang, P.-J., and Liu, J. (2013) Separation of short single- and double-stranded DNA based on their adsorption kinetics difference on graphene oxide. *Nanomaterials 3*, 221−228.
(48) Robertson, N. M., and Yigit, M. V. (2014) The role of microRNA in resistance to breast cancer therapy. *Wiley Interdiscip. Rev. RNA 5*, 823−833.
(49) Zagorodko, O., Spadavecchia, J., Serrano, A. Y., Larroulet, I., Pesquera, A., Zurutuza, A., Boukherroub, R., and Szunerits, S. (2014) Highly sensitive detection of DNA hybridization on commercialized graphene-coated surface plasmon resonance interfaces. *Anal. Chem. 86*, 11211−11216.
(50) Liu, J. (2012) Adsorption of DNA onto gold nanoparticles and graphene oxide: surface science and applications. *Phys. Chem. Chem. Phys. 14*, 10485−10496.
(51) Jang, H., Ryoo, S. R., Lee, M. J., Han, S. W., and Min, D. H. (2013) A new helicase assay based on graphene oxide for anti-viral drug development. *Mol. Cells 35*, 269−273.
(52) Zhou, Z., Zhu, C., Ren, J., and Dong, S. (2012) A graphene-based real-time fluorescent assay of deoxyribonuclease I activity and inhibition. *Anal. Chim. Acta 740*, 88−92.
(53) Takeshita, H., Nakajima, T., Mogi, K., Kaneko, Y., Yasuda, T., Iida, R., and Kishi, K. (2004) Rapid quantification of DNase I activity in one-microliter serum samples. *Clin. Chem. 50*, 446−448.
(54) Ramsey, B. W. (1996) Management of pulmonary disease in patients with cystic fibrosis. *N. Engl. J. Med. 335*, 179−188.
(55) Cui, L., Lin, X., Lin, N., Song, Y., Zhu, Z., Chen, X., and Yang, C. J. (2012) Graphene oxide-protected DNA probes for multiplex microRNA analysis in complex biological samples based on a cyclic enzymatic amplification method. *Chem. Commun. 48*, 194−196.

DOI: 10.1021/acs.bioconjchem.5b00067
Bioconjugate Chem. 2015, 26, 735−745